UHF Micromechanical Compound-(2,4) Mode Ring Resonators With Solid-Gap Transducers

Li-Wen Hung and Clark T.-C. Nguyen
Department of Electrical Engineering and Computer Science
University of California at Berkeley
Berkeley, CA 94720 USA

Yuan Xie, Yu-Wei Lin, Sheng-Shian Li, and Zeying Ren
Department of Electrical Engineering and Computer Science
University of Michigan
Ann Arbor, MI 48109 USA

***Abstract*— UHF vibrating micromechanical ring resonators with solid-filled dielectric transducer gaps (as opposed to previous air gaps) operating in a compound-(2,4) mode have been demonstrated at 979.6 MHz with *Q*'s on the order of 3,100 and motional resistances effectively 4.7× smaller than air gap counterparts under identical bias conditions. Due to their higher dielectric constant, substitution of solid dielectric materials for air or vacuum in the electrode-to-resonator gap leads to increased electromechanical coupling in capacitively transduced micromechanical resonators, which in effect generates more output current, and thus, reduces motional resistance. The advantages of using solid dielectric material as the 'gap' are multifold, as it (1) eliminates the need for the final gap release etch in the MEMS fabrication process, thereby enhancing yield; (2) lowers device impedance versus air gap renditions, allowing easier matching to other components; (3) eliminates the possibility of particles getting into an electrode-to-resonator air gap, which would otherwise pose a potential reliability issue; and (4) consolidates the resonator structure, making it less susceptible to shock. This work greatly extends the frequency of direct (as opposed to indirect) solid-gap transduced MEMS resonators, from the previous 60 MHz using a compound (2,1) mode, to now nearly 1 GHz, and in a range desired for RF front ends, using a compound (2,4) mode.**

***Index Terms*—microelectromechanical devices, microresonator, solid-gap transducer, impedance, quality factor, high frequency.**

I. Introduction

Polysilicon capacitively-transduced vibrating micromechanical resonators have so far posted the highest GHz-range on-chip *Q*'s, in excess of 15,000 at 1.46 GHz [1]. However, their relatively high impedances still encumber them in the eyes of RF designers, who generally look to match to the popular 50Ω of mainstream convention. Given the loss advantages of systems based on higher matching impedances, where matching impedances much larger than parasitic resistances allow lower overall losses than lower impedance systems, it would not be surprising if 50Ω systems are soon replaced by higher impedance ones, especially as more components move on-chip, where impedance conventions no longer matter. Still, if impedances do rise, they likely will not rise past the single-digit kΩ range, beyond which parasitic capacitance can limit the system bandwidth if not inductively cancelled or otherwise suppressed. Thus, although 50Ω will likely not ultimately be necessary, a reduction of the impedances of GHz capacitively-transduced micromechanical resonators down to the kΩ range is desirable.

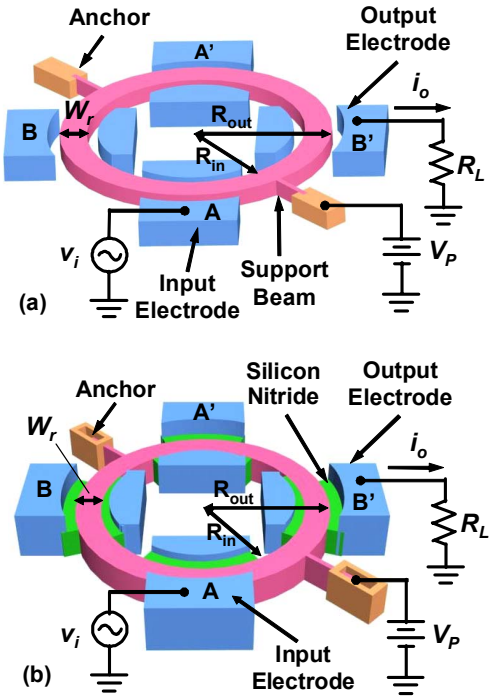

Fig. 1: Perspective-view schematic of (a) an air-gap micromechanical extensional wine-glass ring resonator; and (b) a solid-dielectric version, both in their typical bias and excitation configurations. Note that in both cases, each output electrode is connected to its corresponding inner electrode. Electrodes A and A', electrodes B and B' are usually electronically connected to serve as input and output electrode, respectively.

One effective method for lowering impedance entails the use of solid-dielectric material in the electrode-to-resonator gap to increase the permittivity, thereby increase both the drive force and the output current of a given device, provided the *Q* and amplitude of motion are not reduced too much in the process. Two approaches to solid-gap capacitive transduction have been demonstrated previously: one where direct lateral transduction is used, where lateral forces induce lateral vibrations [2]; and one where an indirect vertical-to-lateral mechanism is employed, where vertical forces squeeze a structure to induce a lateral resonance motion [3]. To date, the latter has achieved the lowest frequency-impedance products, on the order of (809.1MHz) × (59Ω) = 4.8×10^4 MHz-Ω

This work was supported by DARPA.

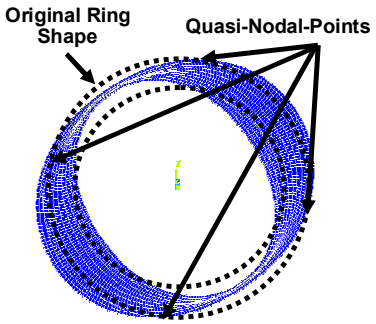

Fig. 2: ANSYS-simulated resonance vibration mode shape for an extensional wine-glass mode ring resonator.

when using HfO_2 as the dielectric material. The former has so far only been demonstrated using silicon nitride dielectric material, so has not achieved as low an impedance, but has achieved the highest Q's, in excess of 20,200 at 160 MHz.

To further explore the efficacy of the lateral solid-gap approach at near GHz frequency, this work applies lateral nitride solid gaps to a UHF vibrating micromechanical ring resonator operating in a compound-(2,4) mode, previously dubbed the extensional wine-glass mode in [4], and compared with an air-gap version in Fig. 1. The demonstrated device vibrates at 979.6 MHz with Q's on the order of 3,100 on par with previous air-gap versions, and with motional resistances R_x effectively 4.7× smaller. Although this reduction factor is somewhat short of expectations, and the demonstrated device could benefit from the use of higher-k dielectric materials to increase the reduction factor, this work still greatly extends the frequency range of direct (as opposed to indirect) solid-gap capacitively transduced MEMS resonators from the previous 160 MHz using a compound (2,1) mode [2] to now nearly 1 GHz, and in a range desired for RF front ends, using a compound (2,4) mode.

II. Structure and Operation of the Extensional Wine Glass Ring Resonator

The compound (2,4) mode ring resonator of this work, shown in Fig. 1 and first demonstrated in [4], is composed of a 2μm-thick ring structure with an inner radius R_{in} of 36.8μm and an outer radius R_{out} of 50μm. Four pairs of electrodes surround the inside and outside of the ring, with each electrode pair occupying one of four ring quarters defined by support beams attached at the quasi-nodal points of the compound-(2,4) mode, shown in Fig. 2. In this mode shape, the widths of two diagonal ring quarters expand along one axis, while the other two compress along the orthogonal axis. To effect a "solid-gap" capacitive transducer, the electrode-to-resonator gaps are filled with solid silicon nitride, deposited 28-nm thick via low-pressure chemical vapor deposition (LPCVD) at 800°C.

The resonance frequency for the extensional wine-glass ring with solid electrode-to-resonator gaps generally ends up being very close to that of its air-gap counterpart. Ignoring the effect of V_P-induced electrical stiffness [5], the resonance frequency f_o for an extensional wine-glass mode ring resonator is given by

$$f_o = \frac{h}{2\pi}\sqrt{\frac{E}{\rho(1-\sigma^2)}} \tag{1}$$

where ρ, σ, and E are the density, Poisson ratio, and Young's modulus, respectively, of the ring structural material, and h is a parameter that depends (among other things) upon the inner and outer radius, R_{in} and R_{out}, respectively, of the ring, shown in Fig. 1, and on the order of the vibration mode shape.

The resonance frequency of an extensional wine-glass ring is most accurately specified by (1). But considering that the extensional wine-glass mode is comprised largely of expansion and contraction about the ring width, which is similar to the longitudinal vibration of a bar, the resonance frequency can be approximately specified by

$$f_{o|approx.} = \frac{m}{2W_r}\sqrt{\frac{E}{\rho}},\ m = 1,3,5,\cdots, \tag{2}$$

where $W_r = (R_{out} - R_{in})$ is the ring width, shown in Fig. 1, and m is the order of the vibration mode. The strong dependence in (2) on the lateral dimension W_r means the frequency of the device can be specified via mere CAD layout, which in turn means that many different frequency resonators can be fabricated onto a single chip in one structural film—a major advantage over many UHF resonators used today, for which frequencies are determined primarily by thickness, which cannot be specified via CAD layout.

To excite the device, a dc-bias voltage V_P is applied to the conductive ring and an ac voltage v_i to input electrodes. Together, these voltages generate an AC electrical force that drives the device into resonance vibration if the frequency of v_i matches the resonance frequency f_o. Once vibrating, the ensuing dc-biased time varying electrode-to-resonator capacitors generate output currents that, when plotted versus the frequency of the input, trace out the desired high-Q bandpass biquad transfer function.

III. Efficacy of a Solid-Gap Transducer

The motional resistance of a capacitively transduced micromechanical resonator is generally given by the expression

$$R_x = \frac{k_r}{\omega_o Q V_P^{\,2}}\cdot\left[\frac{\partial C}{\partial x}\right]^{-2} \cong \frac{k_r}{\omega_o Q V_P^{\,2}}\cdot\frac{d_o^{\,4}}{\varepsilon_r^{\,2}\varepsilon_o^{\,2}A_o^{\,2}} \tag{3}$$

where on the left hand side k_r is the effective stiffness of the disk; $\omega_o = 2\pi f_o$ is the radian resonance frequency; V_P is the DC-bias; and $\partial C/\partial x$ is the change in resonator-to-electrode capacitance per unit displacement, which due to the non-uniform extensional wine-glass mode shape in electrode overlap regions, requires integration to accurately specify [6]. An approximation to its value, however, can be obtained by ignoring the mode shape, which then yields the rightmost expression of (3), where A_o and d_o are the electrode-to-resonator overlap and gap spacing, respectively, of the wine-glass disk resonator; and ε_o and ε_r are the permittivity in vacuum and the relative permittivity of the gap material, respectively.

Equation (3) indicates that there are multiple ways to reduce R_x. As covered in [4], making the ring larger would in-

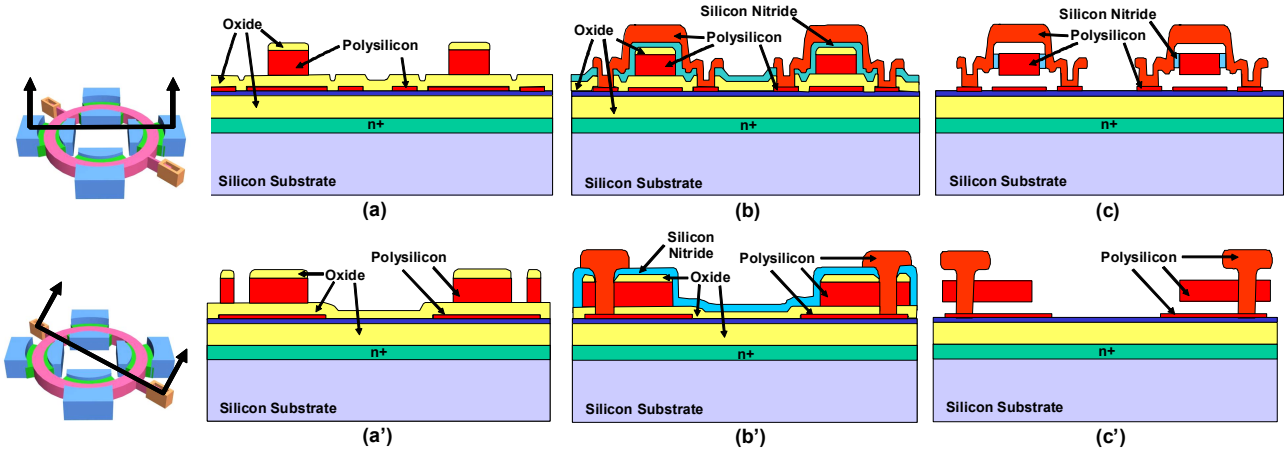

Fig. 3: Cross-sections of the fabrication process flow used for the solid-gap micromechanical extensional wine-glass rings of this work.

crease the overlap area A_o, hence lower R_x, but the degree to which this can be done is limited by the fact that larger rings have a higher tendency to resonate in unwanted spurious modes. Increasing the dc-bias voltage V_P effects a square-law reduction in R_x, but the value of V_P is eventually bounded by pull-in effects [5] or dc supply rails, which are often limited by system considerations. Reducing the disk-to-electrode gap d_o, is appealing because R_x depends on gap distance d_o to the fourth power. The minimum achievable gap distance, however, is limited by the fabrication process technology. In addition, a smaller gap spacing often results in a smaller pull-in voltage, where the resonator pulls in and shorts to an electrode if the applied dc-bias voltage V_P is too large. In the face of these limitations, the use of a dielectric material to raise the gap permittivity ε_r over that of air (or vacuum) presents an attractive method for reducing R_x.

From (3), R_x clearly decreases via ε_r^2, which means it can decrease faster than the electrode-to-resonator overlap capacitance C_o increases as long as no other parameters in the R_x expression cause an offsetting increase in its value. The parameters most likely to counteract the decreasing action of ε_r^2 and raise R_x are: the Q, which can degrade due to increased dissipation in the solid dielectric layer or its interfaces with the adjacent disk and electrode sidewalls; and the effective stiffness k_{tot}, which increases if introduction of the solid-gap attenuates the vibration amplitude of the resonator to a value below the air-gap case.

From (3), if the decrease in motional resistance R_x attained via introduction of a solid gap does not outpace the increase in overlap capacitance (or more importantly, the decrease in capacitive impedance $(\omega_o C_o)^{-1}$), the design of some applications becomes difficult. For example, single-ended filters constructed in all conductive materials (e.g., all doped polysilicon) suffer from passband distortion if parasitic currents feeding through the C_o's from input to output rise to magnitudes similar to that of the motional current. Thus, for such all-conductive single-ended capacitively-transduced micromechanical filters, a useful metric that gauges whether or not feedthrough-derived passband distortion is a problem can be defined as the ratio between the motional current magnitude and that of the feedthrough current when there is a direct capacitive path from the input to the output of the filter, which in its simplest form can be written as

$$FOM = \frac{1}{\omega_o C_o R_x} \tag{4}$$

For a solid-gap to be beneficial over an air-gap capacitive transducer, (4) should increase upon introduction of the solid-gap, which means that the motional current increases faster than the feedthrough current.

It should be noted that the choice of (4) as a metric gauging the efficacy of a given capacitive transducer, although convenient and logical for some applications, is not universally relevant. In particular, as shown in [7], a differential mechanical filter is much less susceptible to overlap capacitance C_o than its single-ended counterpart, since it allows for complete cancellation of C_o via inductive resonance. In addition, the feedthrough issue is really only problematic for single-ended filters constructed in all conductive materials, since the feedthrough path can be broken by simply using a non-conductive material somewhere in the filter structure, such as done in [10], where the coupling links were made non-conductive. Furthermore, some oscillator designs, such as the popular Pierce configuration, rely on overlap capacitance to provide phase shifts for proper operation. Thus, although (4) is suggested here as an interesting metric for some single-ended filters, the R_x reduction factor is perhaps still the best metric by which to gauge solid-gap efficacy.

IV. Fabrication Process And Practical Advantages of Solid-Gap Devices

The solid-gap extensional wine-glass ring resonators of this work were fabricated using the process flow of [8], which is summarized via the cross-sections of Fig. 3. The fabrication process starts with n+ doping of a silicon wafer to form a ground plane that helps to suppress feedthrough during testing [8]. This is followed by subsequent low-pressure chemical vapor depositions (LPCVD's) of 2 μm oxide and 300 nm nitride as electrical isolation layers. Next, vias for electrical contacts to the n+ layer are dry etched through the nitride and oxide in places not shown in the cross section. A first layer of polysilicon is then deposited, n+ $POCl_3$-doped, and patterned, to form electrical interconnects and device-specific ground

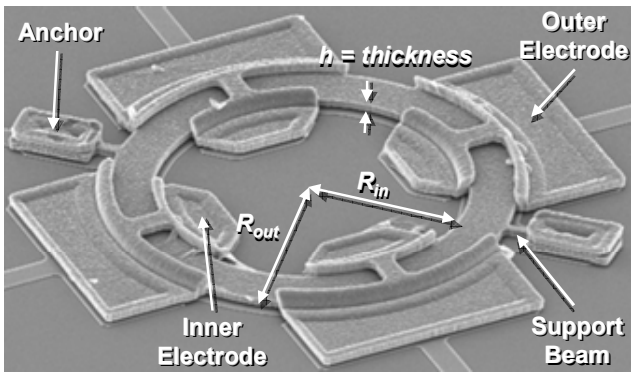

Fig. 4: SEM of a fabricated extensional wine-glass ring resonator.

planes. Successive depositions of 750 nm of a sacrificial oxide, 2 µm of structural polysilicon to later form the resonator structure, and 1.2 µm of oxide to serve as an etch hard mask, are then deposited via LPCVD. (The polysilicon is $POCl_3$-doped to n+ before depositing the oxide hard mask.) The oxide hard mask is patterned to the geometry of the polysilicon ring via lithography and dry etching. Vias for the stems that anchor the ring support bases to the substrate are also etched during this step, using the same mask, which effectively self-aligns the anchor stems to the ring. The ring and stem via patterns are then transferred to the polysilicon ring via etching, using the oxide as a hard mask. At this point in the process, the cross-section looks as in Fig. 3 (a) and (a′).

To define the electrode-to-resonator gap, a thin film is next deposited conformally over the whole wafer, and most importantly along the sidewalls of the ring, to a thickness equal to the desired electrode-to-resonator gap spacing. For an air-gap device, this layer is LPCVD high temperature oxide (HTO) deposited at 920°C, which can be removed along with all the other sacrificial oxides during the hydrofluoric acid (HF) release step at the end of the process. For the present solid-gap devices, the deposited film is silicon nitride, which stays intact during the HF release step. After formation of sidewall spacers, a third layer of polysilicon is deposited 2 µm-thick, n+ $POCl_3$-doped, and patterned to form inner and outer electrodes, after which the process cross-sections look as in Fig. 3 (b) and (b′). The structures are finally released in the aforementioned HF release step, where again, the sidewall spacer is removed for air-gap devices, but stays intact for solid-gap devices, leaving the final cross-section shown in Fig. 3 (c) and (c′).

The main difference in the fabrication sequence between air-gap and solid-gap devices is simply that the electrode-to-resonator gap material must be removed for air-gap, but not for solid-gap. This turns out to be a major advantage for solid-gap devices, and possibly the most important one. Specifically, the most difficult step in a small lateral air-gap process is removal of the sacrificial sidewall spacer material that defines the gap, since HF might have difficulty getting into the tiny gaps, and etch by-products might block it from getting all the way through. The smaller the air-gap, the more difficult is the release process, hence the lower the yield of functional devices. In contrast, the described solid-gap process has the distinct advantage of not requiring a gap release,

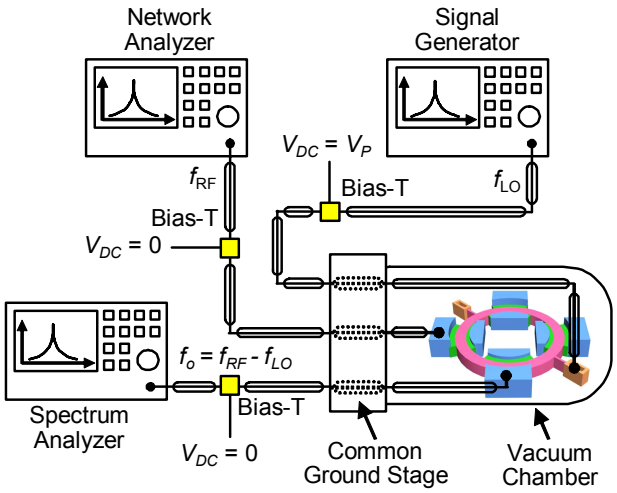

Fig. 5: Pictorial description of the mixing method used for measurement of solid-gap wine-glass ring resonators.

so it not only allows a higher yield, but can also achieve much thinner solid-filled gaps, on the order of 28nm versus the 65nm often used for air-gap devices. In addition, finished solid-gap devices are more robust than air gap devices, since they are better stabilized against shock, and they do not suffer from gap contamination issues, where particles or moisture might get into the electrode-to-resonator gap.

V. Experimental Results

Both solid-gap and air-gap (for comparison) devices were fabricated using appropriate versions of the process flow in Fig. 3. Fig. 4 presents the SEM of a completed 980-MHz extensional wine-glass ring.

A. Measurement Strategy

As mentioned above, the increased permittivity of a solid-gap capacitively transduced resonator generates significantly larger electrode-to-resonator overlap capacitance C_o than typically present for air-gap devices. Although the C_o's of the direct lateral devices of this work are generally much smaller than those of vertical-to-lateral types [3], they might still encumber measurement of devices if the motional resistance R_x reduction attained via use of solid-gaps is smaller than the decrease in $(\omega_o C_o)^{-1}$. In differential devices [7], this capacitance can be resonated out via an inductive or more functional *LC*-based frequency shaping circuit. For such differential mechanical circuits, larger values of C_o can even be beneficial, since this would permit the use of smaller resonating inductance values, such as the 3-5 nH commonly available on-chip in conventional CMOS technology.

For single-ended devices, however, inductive resonance cancellation is not as simple to implement, since finite interconnect resistance prevents an added inductor from resonating out all the C_o capacitance [7]. Thus, for the present effort, rather than resonate out potentially large solid-gap C_o's, it is simpler and more convenient to just separate the motional currents of main interest from the parasitic feedthrough currents induced by C_o.

In this work, the mixing method of [9], shown in the schematic of Fig. 5, is used to separate motional currents

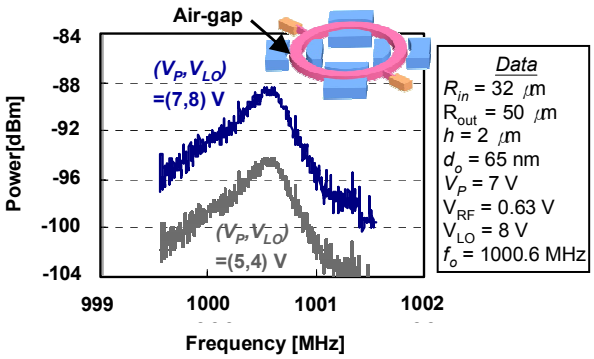

Fig. 7: Measured frequency response of a 1000.6-MHz air-gap micromechanical wine-glass ring resonator.

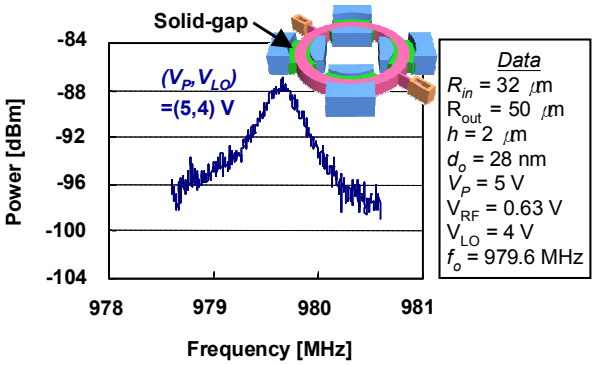

Fig. 6: Measured frequency response of a solid-gap 979.6-MHz micromechanical wine-glass ring resonator.

from feedthrough currents in the frequency domain. Here, the application of a local oscillator (LO) to the resonator structure allows the resonator to be driven via a radio frequency (RF) signal that mixes with the LO via nonlinearity in the capacitive transducer, thereby generating a force component at the difference frequency, ω_{RF}-ω_{LO}. When ω_{RF}-ω_{LO}=ω_o, the resonance frequency of the ring, the ring vibrates at ω_o, generating a motional current at ω_o widely separated from feedthrough at the RF and LO frequencies. This then allows a spectrum analyzer operating in MAX HOLD mode to detect resonance motional currents all by their lonesome, without interference from feedthrough. Resonator frequency characteristics obtained in this manner are thus quite clean, allowing a very accurate determination of the degree of R_x reduction provided by solid-gap transducers, plus a very accurate measurement of the actual mechanical Q of the device under test.

It should be noted that mixing measurement is only a characterization method. In an actual application, unless the device in question is a mixler [10], devices are not operated in this way. In particular, a filter utilizing resonators like these must be properly terminated and measured directly, not via mixing, since this is how it would be used in the actual application. For this work, however, mixing is quite appropriate for solid-gap resonator characterization, since it yields much more accurate results.

B. Measurement Results

Each measured sample was prepared by first attaching a die containing devices onto a custom-built test board and bond wiring device pads to appropriate metal interconnect traces on this board. To enable vacuum measurements, the test board was then inserted into a custom-built vacuum chamber that allowed connection of test board I/O ports through the vacuum interface to measurement instrumentation on the outside.

Fig. 6 and Fig. 7 present frequency characteristics measured in vacuum using the mixing set-up of Fig. 5 for air-gap and nitride-gap versions, respectively, of extensional wine-glass rings, like that shown in Fig. 4. Because the output in the measurement setup is sensed by a spectrum analyzer in MAX HOLD mode, these frequency plots represent only the raw output of the resonator power attenuated by the impedance mismatch between the resonator and the 50Ω input of the spectrum analyzer. This explains the dBm units on the y-axis. The somewhat very low values of dBm are caused by a rather large impedance mismatch between the measured devices and 50Ω.

The two resonators measured here are identical, except the one in Fig. 6 has a 65 nm air gap, and the one in Fig. 7 has a 28 nm nitride gap. Immediately apparent is that their resonance frequencies, at 1000.6 MHz and 979.6 MHz, respectively, are quite close, and this facilitates the prediction of frequency for the solid-gap device. Interestingly, the 3,160 Q of the solid-gap device is actually higher than the 2,200 of the air-gap device—something that presently eludes rigorous explanation, but which might be attributable to simple process-related variance in device Q's. More data on these devices are needed to determine statistical characteristics, such as mean and standard deviation, before any concrete conclusions can be made, here. However, the fact that the Q of the solid-gap device is on par with that of the air gap, is at least encouraging. However, the Q less than 10,000 for both, although sufficient for pre-select filters, is not sufficient for RF channel-selection [11], so is somewhat disappointing. Further study is needed to isolate the cause of the lower Q, which quite possibly might just be a peculiarity of this specific process run.

For fair comparison of motional resistance, the data for the air-gap device, originally taken with V_P=7V and V_{LO}=8V, was adjusted using known (and proven) dependencies on dc-bias and local oscillator amplitude to allow a direct comparison under the same bias conditions between the two devices, with V_P=5V and V_{LO}=4V. After the adjustment, a decrease in solid-gap R_x (versus air-gap) of 4.7× is seen, which is good, but disappointing, since this is smaller than the permittivity increase of 7.8×, meaning that for this particular 980-MHz device, the C_o capacitance increased faster than the motional resistance R_x decreased when the nitride gap was introduced, making an all-polysilicon single-ended version of this device more susceptible to feedthrough than its air gap counterpart. Even worse, the FOM value is 5.4×10^{-4} for the air gap device, and 1.4×10^{-4} for the nitride-gap device, further indicating that the introduction of the nitride-gap was not beneficial from a performance perspective, at least for all-conductive single-ended devices.

Thus, at least in this instance, the introduction of solid-gap capacitive transducers did not improve the FOM. In fact, if an air-gap device with the same 20 nm gap as the solid-gap

device were achievable, theory predicts that the air-gap device would far outperform the measured solid-gap one, in both R_x and FOM. It appears that the need to compress and expand the solid nitride gap layer has a more encumbering effect on the present devices than on previous wine-glass disks [2], as might be expected when considering that the ring frequencies are quite different from the wine-glass disks, so the wavelength-optimized gap-electrode thickness needed to maximize the edge-to-edge displacement of the solid-gap is different.

Although an FOM improvement was not observed, here, the other benefits of solid-gap transduction were still seen, such as higher fabrication yield and greater motional current (than the achievable 65 nm air-gap version). For differential or partially non-conductive mechanical filters [7], and for oscillators, these are more important than the FOM, so the use of nitride-gaps does prove quite useful for these applications. To attain even greater reductions in R_x, gap materials with much higher permittivity than silicon nitride are attractive, such as HfO_2 or Barium Strontium Titanate (BST). Work to incorporate these is in progress.

VI. Conclusions

UHF vibrating micromechanical ring resonators with solid-filled dielectric transducer gaps (as opposed to previous air gaps) operating in a compound-(2,4) mode have been demonstrated at 979.6 MHz with Q's on the order of 3,100 and motional resistances 4.7× smaller than air gap counterparts under identical bias conditions. This work greatly extends the frequency of direct (as opposed to indirect) solid gap transduced MEMS resonators, from the previous 60 MHz using a compound (2,1) mode, to now nearly 1 GHz, and in a range desired for RF front ends, using a compound (2,4) mode. However, the performance enhancement afforded by solid-gap capacitive transducers in this work was somewhat less than desired, since the reduction factor attained for motional resistance was smaller than the factor by which the electrode-to-resonator overlap capacitance increased, and this can be problematic for some single-ended (as opposed to differential) applications of micromechanical resonators. To remedy this, work towards optimizing the solid-gap material type and thickness to allow maximum gap material expansion and contraction is ongoing.

Acknowledgment: This work was funded by DARPA.

References

[1] S.-S. Li, Y.-W. Lin, Y. Xie, Z. Ren, and C. T.-C. Nguyen, "Micromechanical hollow-disk ring resonators," *Proceedings*, IEEE Int. MEMS Conf., Maastricht, The Netherlands, Jan. 25-29, 2004, pp. 821-824.

[2] Y.-W. Lin, S.-S. Li, Y. Xie, Z. Ren, and C. T.-C. Nguyen, "Vibrating micromechanical resonators with solid dielectric capacitive transducer gaps," *Proceedings*, Joint IEEE Int. Frequency Control/Preciison time & time Interval Symposium, Vancouver, Canada, Aug. 29-31, 2005, pp. 128-134.

[3] H. Chandrahalim, d. Weinstein, L.-F. Cheow, and S. A. Bhave, "Channel-select micromechanical filters using high-k dielectrically transduced MEMS resonators," *Proceedings*, IEEE Int. Conf. Micro-Electro-Mechanical Systems, Istanbul, Turkey, Jan. 22-26, 2006, pp. 894-897.

[4] Y. Xie, S.-S. Li, Y.-W. Lin, Z. Ren, and C. T.-C. Nguyen, "UHF micromechanical extensional wine-glass mode ring resonators," *Technical Digest*, IEEE Int. Electron Devices Meeting, Washington, DC, Dec. 8-10, 2003, pp. 953-956.

[5] H. Nathanson, W. E. Newell, R. A. Wickstrom, and J. R. Davis, Jr., "The resonant gate transistor," *IEEE Trans. Electron Devices*, vol. ED-14, No. 3, pp. 117-133, March 1967.

[6] Y.-W. Lin, S. Lee, S.-S. Li, Y. Xie, Z. Ren, and C. T.-C. Nguyen, "Series-resonant VHF micromechanical resonator reference oscillators," *IEEE J. Solid-State Circuits*, vol. 39, no. 12, pp. 2477-2490, Dec. 2004.

[7] S.-S. Li, Y.-W. Lin, Z. Ren, and C. T.-C. Nguyen, "An MSI micromechanical differential disk-array filter," *Tech. Digest*, *Dig. of Tech. Papers*, the 12th Int. Conf. on Solid-State Sensors & Actuators (Transducers'07), Lyon, France, 2007, pp. 307-312.

[8] J. Wang, Z. Ren, and C. T.-C. Nguyen, "1.156-GHz self-aligned vibrating micromechanical disk resonator," *IEEE Trans. Ultrason., Ferroelect., Freq. Contr.*, vol. 51, no. 12, pp. 1607-1628, Dec. 2004.

[9] J. Wang, J. E. Butler, T. Feygelson, and C. T.-C. Nguyen, "1.51-GHz polydiamond micromechanical disk resonator with impedance-mismatched isolating support," *Proceedings*, MEMS'04, Maastricht, The Netherlands, Jan. 2004, pp. 641-644.

[10] A.-C. Wong and C. T.-C. Nguyen, "Micromechanical mixer-filters ("mixlers")," *IEEE/ASME J. Microelectromech. Syst.*, vol. 13, no. 1, pp. 100-112, Feb. 2004.

[11] C. T.-C. Nguyen, "MEMS technology for timing and frequency control," *IEEE Trans. Ultrason., Ferroelect., Freq. Contr.*, vol. 54, no. 2, pp. 251-270, Feb. 2007.